Modeling Biofilm Accumulation and Mass Transport in a Porous Medium Under High Substrate Loading

O. Wanner
Department of Computer and System Sciences, Swiss Federal Institute, for Environmental Science and Technology (EAWAG), CH- 8600 Duebendorf, Switzerland

A. B. Cunningham* and R. Lundman
Center for Biofilm Engineering, Montana State University, Bozeman Montana, 59717

Received January 16, 1995/Accepted April 26, 1995

A packed bed biofilm reactor inoculated with pure culture *Pseudomonas aeruginosa* was run under high substrate loading and constant flow rate conditions. The 3.1-cm-diameter cylindrical reactor was 5 cm in length and packed with 1-mm glass beads. Daily observations of biofilm thickness, influent and effluent glucose substrate concentration, and effluent dissolved and total organic carbon were made during the 13-day experiment. Biofilm thickness appeared to reach quasi-steady-state condition after 10 days. A published biofilm process simulation program (AQUASIM) was used to analyze experimental data. Comparison of observed and simulated variables revealed three distinct phases of biofilm accumulation during the experiment: an initial phase, a growth phase, and a mature biofilm phase. Different combinations of biofilm and mass transport process variables were found to be important during each phase. Biofilm detachment was highly correlated with shear at the biofilm surface during all three phases of biofilm development.
Key words: biofilm modeling • detachment • porous media • biobarriers

INTRODUCTION

The rate and extent of biofilm accumulation in porous media systems is of concern to the design and operation of packed bed reactors used for water treatment as well as in subsurface injection systems which are concerned with in situ bioremediation, enhanced oil recovery, and groundwater recharge.[6,10,12] In these systems, bacteria attach to the solid phase by means of a matrix of polysaccharides that extend from the cell and form a mass of tangled fibers. The cells, polysaccharide material, together with solid particles filtered from the bulk fluid comprise the biofilm matrix.[3]

In this article "high substrate loading" refers to the condition whereby substrate supply to the biofilm is sufficient to permit the formation of thick, continuous biofilms, as opposed to patchy, isolated cell colonies. The relationship between substrate loading rate and biofilm morphology is discussed in detail by Rittmann.[15] Under high substrate loading conditions, the average biofilm thickness on individual media particles will increase, resulting in a corresponding decrease in effective pore space.[7] In systems where the flow rate through the porous media remains constant, the average pore velocity will increase with the increasing biofilm thickness, while in systems where the piezometric gradient remains constant, pore velocity will decrease. Increased thickness may result in depletion of nutrients within the biofilm structure. It is probable that the net rate of biofilm detachment increases with increasing biofilm thickness; however, additional research is needed to fully confirm that assumption. However, it is clear that as the temporal progression of biofilm thickness reaches a quasi-steady-state condition, the average specific growth rate for the biofilm must be balanced by the net detachment rate.[20]

The accumulation and activity of biofilms varies from point to point along individual porous media pore channels and thus are considered to be microscale phenomena. Ideally, mechanistic modeling should likewise be carried out at the microscale in order to completely describe these processes. However, mathematical simulation of biofilm processes at the individual pore channel scale represents a major computational challenge, and development and evaluations of such models are just beginning.[4]

If bulk media properties and Darcian flow are assumed along with other traditional concepts in porous media modeling, the modeling approach is simplified. The concepts of advection, dispersion, and sorption, together with Darcy's law and conservation equations, are usually adequate to describe flow and nonreactive mass transport through porous media. Chemical reactions in the liquid phase as well as reactions between chemical species dissolved in the liquid phase and species sorbed to the solid matrix of the porous medium have successfully been incorporated into these models. Examples of studies involving transport-biofilm model development and evaluation have been reported by Rittmann and McCarty,[16] Taylor and Jaffe,[19] and Saez and Rittmann.[18] The question addressed by this article is whether coupled porous media transport-biofilm models can be extended and applied to a situation in which, under

* To whom all correspondence should be addressed.

CCC 0006-3592/95/060703-10

high substrate loading, biomass accumulates so as to occupy a significant portion of the free pore space.

The biofilm modeling approach of Gujer and Wanner[9] and the AQUASIM program provide the basis for this investigation. AQUASIM is well documented[13,14] and has been previously used to analyze various biofilm systems, including river beds, and surfaces of tanks and conduits. Our investigation has determined that AQUASIM can also be used to effectively model biofilm accumulation and activity in saturated porous media.

MATERIALS AND METHODS

Materials

The experimental system consisted of a 50-mm cylindrical reactor containing 1-mm glass beads. The 31-mm-diameter reactor housing was chosen to give a ratio of housing diameter to particle diameter of at least 30:1, which is the minimum ratio recommended by Cohen and Metzner[5] for laminar flow that will allow wall effects on packing and fluid flow to be neglected. The glass beads were contained in the reactor by No. 30 brass gauze mesh over each end of the glass tubing. The flow was dispersed by funnels attached to each end of the reactor with silicon sealant. Pressure taps, sampling ports, and conductivity probe ports were provided at each end of the reactor at the gauze–media interface. All the tubing used in the experiment was Masterflex silicone (oxygen-permeable) tubing. The pumps used were Masterflex peristaltic pumps.

The biofilm was developed using a *Pseudomonas aeruginosa* inoculum and an influent glucose concentration which varied between 7 and 16 g C m^{-3}. The composition of the nutrient solution was the same as that reported by Cunningham *et al.*[7] Distilled (aerated) water from an elevated storage reservoir was filtered through two 0.2-μm cartridge filters in series. This sterile dilution water then passed through a stainless steel coil submerged in a constant temperature water bath to ensure a constant operating temperature of 20°C. A flow break was included to prevent regrowth. Nutrients were added upstream of the flow break. An injection port for the salt tracer was located approximately 15 cm ahead of the reactor.

The nutrients were separated into two feed tanks to prevent contamination. The phosphates and glucose were isolated from other minerals in an attempt to produce a nutrient limited environment in both containers. Although the temperature of the minerals and substrate were not controlled, they were mixed with the dilution water in a 1:100 volume ratio and thus their effect on the fluid temperature was considered negligible.

System Operation

Prior to startup, the entire system was autoclaved at 18 psig and 125°C for 1 h. The nutrient tanks required autoclaving overnight due to the large amount of liquid present. The reactor was inoculated with a *P. aeruginosa* inoculum grown aerobically in batch culture at 35°C for approximately 2 days. The inoculum concentration was approximately 10^7 cells/mL.

During inoculation the reactor was isolated using hose clamps, filled with inoculum through the upstream sampling port, and allowed to stand for 4 h to allow for bacterial attachment to the media surfaces. The hose clamps were subsequently removed and the system was operated at a constant flow rate of 38 ML/min.

Variables measured during the experiment included total organic carbon (TOC) concentrations, dissolved organic carbon (DOC) concentrations, glucose concentrations, suspended cell concentrations, pressure drop across the reactor, and biofilm thicknesses. A tracer study was also conducted to determine average pore velocity. Total organic carbon, DOC, glucose, and cell concentrations were measured at both the influent and effluent of the reactor.

Analytical Methods

Total organic carbon measurements were made on a Dorhman DC 80 carbon analyzer. Any carbon in the sample is oxidized to carbon dioxide by a potassium persulfate solution in the presence of ultraviolet light. The amount of carbon dioxide evolved by this reaction was then monitored by an infrared gas detector. A computer integrated the reading from the infrared gas detector to give the organic carbon concentration. Samples were first acidified to a pH of 2 to remove any inorganic carbon (e.g., carbonates). Subsequent oxygen purging then removed any carbon dioxide dissolved in the liquid. These preliminary steps were crucial to measurement accuracy as the analyzer cannot distinguish the source of the carbon dioxide. The liquid injection into the DC 80 was manual. Each sample was injected in triplicate.

Dissolved organic carbon samples were centrifuged at 10,000 rpm (rotor radius 14.57 cm, 16,247 g) for 10 min, then processed identically to the TOC samples. This procedure concentrated particulates such as microbial cells in the bottom of the centrifuge tube, leaving only the dissolved carbon in the supernatant. The supernatant was then tested for organic carbon content.

Glucose concentrations were determined calorimetrically using Sigma Diagnostics Enzymatic Glucose Determination (procedure no. 510). This procedure employs two separate enzymatic reactions. In the first reaction, glucose oxidase converts any glucose present into gluconic acid. The second reaction then reacts peroxidase with the gluconic acid to produce *ortho*-dianisidine. The *ortho*-dianisidine is brown in color and can thus be detected using a spectrophotometer. Over a wide range of glucose concentrations the absorbance of the *ortho*-dianisidine is linear with concentrations. Each of these samples was also tested in triplicate. The standard error of estimate (i.e., mean/standard deviation) was ap-

proximately 10% for glucose and 10% for TOC and DOC measurements.

Biofilm thickness measurements were made optically through the glass sides of the reactor. A micrometer was placed in the ocular of the microscope and calibrated for different magnifications. By focusing the microscope on the exposed edge of a bead, the film thickness could then be measured at that point. Ten squares were randomly marked on the outside of the reactor. The thickness measurements were taken inside these boxes. The boxes insured that the location of the measurements were random and consistent so that the measurements would not be influenced by the human attraction to thicker films. This technique only allowed viewing of the outer few layers of beads and film. At least 10 measurements were averaged for each thickness reported. The standard error of estimate for biofilm thickness measurements was approximately 15%. Pressure drop across the reactor was measured using two vertical stand pipes, one at the entrance and one at the exit.

Suspended cells were counted using image analysis techniques. The cells were stained with Hoechst 33342 or DAPI. A known quantity of sample was filtered through a 0.1-mm black polycarbonate membrane filter. The filter paper was placed under a microscope equipped with ultraviolet light and magnified 1500 times.

A computer processed the image from a video camera. Once calibrated to record only objects of the same size and color as cells, the computer could count the number of such objects in the field. The counting procedure was repeated until approximately 10 fields or 300 cells had been imaged. By knowing the area of the field, the area of the filter paper, and the amount of original sample that was filtered, a number of cells per unit volume could be calculated for the original sample.

Average pore velocity was measured using a sodium chloride tracer. Conductivity probes were placed at the influent and effluent of the reactor. A small quantity of saturated salt solution (filter sterilized) was injected at the injection port upstream from the reactor. As the salt passed the probes, the increase in conductivity of the solution due to the salt ions was recorded by a computer data acquisition system as an increase in a voltage signal. A minimum of three breakthrough curves were recorded per sampling.

MODELING

Using a continuum approach and observing conservation of mass principles, Wanner and Gujer[22] developed a mathematical model to describe microbial interactions in biofilms. The mathematical model used in our article paper was developed in a similar manner.

Biochemical Reactions

The *P. aeruginosa* utilizes glucose and dissolved oxygen to produce cellular mass and extracellular polymeric substances (eps). The production of cellular mass is modeled as

$$r_{psa} = \mu_{max} \frac{C_{glu}}{K_{glu} + C_{glu}} \frac{C_{O_2}}{K_{O_2} + C_{O_2}} X_{psa} \quad (1)$$

where r_{psa} is the production rate ($ML^{-3}t^{-1}$), μ_{max} is the maximum specific growth rate (t^{-1}) and X_{psa} is the concentration (ML^{-3}) of *P. aeruginosa*, C_{glu} is the concentration (ML^{-3}) and K_{glu} is the half-saturation constant (ML^{-3}) of *P. aeruginosa* with respect to glucose, and C_{O_2} is the concentration (ML^{-3}) and K_{O_2} is the half-saturation constant (ML^{-3}) of *P. aeruginosa* with respect to dissolved oxygen. The synthesis of eps is assumed to be associated with cellular growth and is described as

$$r_{eps} = k \cdot r_{psa} \quad (2)$$

where r_{eps} is the eps production rate ($ML^{-3}t^{-1}$) and k is a stoichiometric factor ($M_{eps}M_{psa}^{-1}$). Glucose and oxygen are utilized for both the production of cellular mass and eps. Their utilization rates are given by

$$r_{glu} = \left(- \frac{1}{Y_{psa/glu}} - \frac{k}{Y_{eps/glu}} \right) r_{psa} \quad (3)$$

and

$$r_{O_2} = \frac{1}{i_1} r_{glu} \quad (4)$$

where r_{glu} ($ML^{-3}t^{-1}$) and r_{O_2} ($ML^{-3}t^{-1}$) are the utilization rates of glucose and of dissolved oxygen, respectively, $Y_{psa/glu}$ and $Y_{eps/glu}$ are the observed yield coefficients ($M_{psa}M_{glu}^{-1}$ and $M_{eps}M_{glu}^{-1}$) of the two production processes, and i_1 is a stoichiometric factor ($M_{glu}M_{O_2}^{-1}$). Equation (4) assumes that the total glucose utilization is oxygen dependent. Although alternative formulations are possible, this assumption is based on observations reported by Characklis and Marshall.[3]

Reactor

Mass transport in a cylindrical porous medium reactor usually is described by the one-dimensional advection–diffusion equation. Here the reactor is divided in the axial direction into a number of segments. In each segment a bulk fluid and a biofilm compartment are distinguished. The bulk fluid compartment of a segment is assumed to be well mixed and is modeled by mass balance equations for the components glucose and dissolved oxygen,

$$\frac{d(V_B C_{B,Ci})}{dt} = Q(C_{in,Ci} - C_{B,Ci}) + A_{LF}\, i_{L,Ci} + V_B r_{Ci} \quad (5)$$

and by mass balance equations for the components suspended cells and eps,

$$\frac{d(V_B X_{B,Xi})}{dt} = Q(X_{in,Xi} - X_{B,Xi}) + A_{LF} i_{L,Xi} + V_B r_{Xi} \quad (6)$$

where C_{in} and X_{in} are the segment influent concentrations (ML^{-3}), C_B and X_B are the bulk fluid concentrations (ML^{-3}), i_L is the mass flux per unit surface area across the biofilm–bulk fluid interface ($ML^{-2}t^{-1}$), and r is the net production rate ($ML^{-3}t^{-1}$) of the components C_i and X_i, where V_B is the bulk fluid volume (L^3), Q is the flow rate (L^3t^{-1}) and A_{LF} is the biofilm surface area (L^2) of the segment, and t is time. The interfacial mass flux of dissolved constituents, i_L, is assumed to be given by

$$i_{L,Ci}\lambda = D_{Ci}(C_{L,Ci} - C_{B,Ci}) \tag{7}$$

and

$$i_{L,Xi}\,\lambda = D_{Xi}\,(X_{L,Xi} - X_{B,Xi}) \tag{8}$$

where λ is a mass transfer resistance coefficient (L), D is the molecular diffusivity (L^2t^{-1}), and C_L and X_L and the concentrations (ML^{-3}) of C_i and X_i, respectively, at the bulk fluid side of the biofilm surface. The bulk fluid volume is calculated as

$$V_B = V_C - V_F \tag{9}$$

where V_c is the bulk fluid volume of the reactor (L^3) and V_F is the biofilm volume (L^3).

Biofilm

The reactor wall and the glass beads provide a solid surface to which the microbial cells adhere. The subsequent formation of a biofilm on this surface is described by one-dimensional mass balance equations for cells and eps,

$$\frac{\partial X_{F,Xi}}{\partial t} = -\frac{\partial j_{F,Xi}}{\partial z} + r_{Xi} \tag{10}$$

where X_F is the concentration in the biofilm (ML^{-3}) of the particulate component X_i, Z is the distance perpendicular to the solid surface (L), and i_F is the mass flux in the direction of z ($ML^{-2}t^{-1}$). This biofilm mass flux results from microbial growth and eps production in the biofilm interior and is given as

$$j_{F,Xi} = u_F X_{F,Xi} \tag{11}$$

where u_F is the velocity by which the biofilm solid matrix is expanding (Lt^{-1}). This velocity is calculated as

$$u_F = \frac{1}{1 - \epsilon_l}\int_0^z \left(\frac{r_{psa}}{\rho_{psa}} + \frac{r_{eps}}{\rho_{eps}}\right) dz \tag{12}$$

where ϵ_l is the volume fraction of the liquid phase in the biofilm and ρ_{psa} and ρ_{eps} are the cell and eps densities (ML^{-3}), respectively. The relationship between density and concentration is given by

$$X_{F,Xi} = \rho_{Xi}\epsilon_{s,Xi} \tag{13}$$

where ϵ_s is the volume fraction of the particulate component in the biofilm. The boundary conditions are

$$j_{F,Xi}(z = 0) = 0 \tag{14}$$

at the biofilm–substratum interface and

$$i_{F,Xi} = i_{L,Xi} \tag{15}$$

where i_F is the interfacial mass flux of X_i, at the biofilm side of the biofilm–bulk fluid interface ($ML^{-2}t^{-1}$) and L_F is the biofilm thickness (L). The mass flux i_F is given by

$$i_{F,Xi} = u_{de}X_{F,Xi} \tag{16}$$

where u_{de} is the velocity (Lt^{-1}) by which cells and eps are detached from the biofilm to the bulk fluid. If attachment to the biofilm surface is neglected, progression of the biofilm thickness is modelled by

$$\frac{dL_F}{dt} = u_F\,(z = L_F) - u_{de} \tag{17}$$

Glucose and dissolved oxygen in the biofilm are modeled by the well-known one-dimensional mass balance equation

$$\frac{\partial(\epsilon_l C_{F,Ci})}{\partial t} = -\frac{\partial j_{F,Ci}}{\partial z} + r_{Ci} \tag{18}$$

where C_F is the concentration defined as mass per unit liquid phase volume (ML^{-3}) of the dissolved component C_i. The mass flux is given as

$$j_{F,Ci} = -u_F\,(1 - \epsilon_l)\,C_{F,Ci} - fD_{Ci}\frac{\partial C_{F,Ci}}{\partial z}$$

where D is the molecular diffusivity in pure water (L^2t^{-1}) and f is the ratio of the diffusivities in the biofilm and in pure water. The boundary conditions are

$$j_{F,Ci}\,(z = 0) = 0 \tag{20}$$

$$C_{F,Ci}\,(z = L_F) = C_{L,Ci} \tag{21}$$

and

$$i_{F,Ci} = i_{L,Ci} \tag{22}$$

with the interfacial mass flux of C_i at the biofilm side of the biofilm–bulk fluid interface given as

$$i_{F,Ci} = (-u_F + u_{de}\epsilon_l)\,C_{F,Ci} - fD_{Ci}\frac{\partial C_{F,Ci}}{\partial z} \quad (z = L_F) \tag{23}$$

equations (10)–(23) originate from a mathematical framework for modeling of mixed-culture multisubstrate biofilms which has been developed earlier.[21]

SIMULATION

Simulation Program AQUASIM

For the simulation of the experiment the new computer program AQUASIM was used, which has been designed for the identification and simulation of aquatic systems.[13,14] AQUASIM offers a number of standard compartment types, among them a biofilm reactor compartment, consisting of a

completely mixed bulk fluid zone coupled to a one-dimensional mixed-population, multisubstrate biofilm. The compartments can be connected by advective and diffusive links forming more complex system configurations. Depending on the given initial state, influent concentration time series, and model parameter values, AQUASIM then automatically solves the mass balance equations for all variables in all compartments of the selected configuration and for the kinetic model as specified by the user. The program also includes routines for sensitivity analyses and automatic parameter estimation based on comparison with experimental data.

The simulation performed here was based on Equations (1)–(23) and on three biofilm reactor compartments, of which each represents a segment of the porous medium reactor and is connected to the next compartment by an advective link.

Simulation of Experiment

The model as described above includes 25 parameters. Even though measured time series of four variables are available, these data are by far not sufficient to estimate the values of all model parameters. Thus, the parameters were divided into two groups: a first group of parameters, which are assumed to be given as experimental conditions or to be known a priori from the literature, and a second group with parameter values which are unknown or are of special interest for the system under investigation. The latter group includes the initial biofilm thickness $L_F(0)$, the initial volume fractions of cells, eps and the liquid phase in the biofilm, $\epsilon_{s,psa}(0)$, $\epsilon_{s,eps}(O)$ and ϵ_l, the diffusivities of the suspended cells and the eps in pure water, D_{psa} and D_{eps}, and D_{eps}, the mass transfer resistance coefficient λ and the detachment velocity u_{de} at the biofilm–bulk fluid interface, and the biofilm surface area A_{LF}. The unknown parameters λ, u_{de}, and A_{LF} possibly vary with time or space. Estimates of the values of the unknown parameters were obtained by a simulation using the measured time series of the glucose influent concentration and by a simultaneous fit of the measured time series of glucose, DOC, and TOC in the effluent and of the biofilm thickness.

RESULTS AND DISCUSSION

Experimental and Calculated Time Series

Figure 1 shows the experimental and calculated time series of glucose, DOC, TOC, and the biofilm thickness. In Figure 1a the experimental reactor influent concentrations and the experimental and calculated reactor effluent concentrations of glucose are displayed. The linearly interpolated influent concentrations were used as input for the simulation. Figures 1b, c show the experimental and calculated effluent concentrations of DOC and TOC, respectively. It is assumed that by the centrifugation step of the analytical method used to determine DOC and TOC, microbial cells and eps are separated. Therefore, the calculated values of DOC are equal to the sum of glucose and eps and the calculated values of TOC are equal to the sum of glucose, eps, and *P. aeruginosa* cells. The influent concentrations of

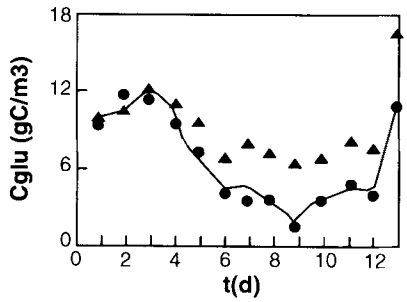

Fig. 1a Glucose concentration

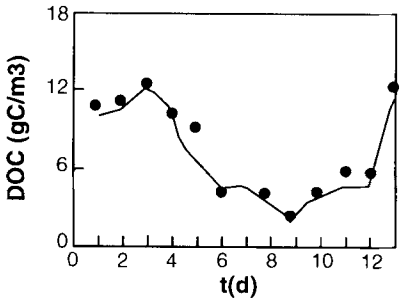

Fig. 1b DOC effluent concentration

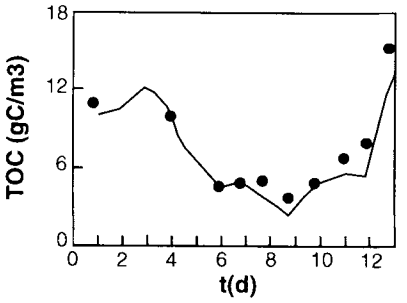

Fig. 1c TOC effluent concentration

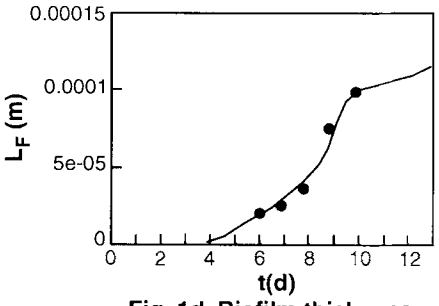

Fig. 1d Biofilm thickness

Figure 1. Observed and predicted time series for glucose (C_{glu}), DOC, TOC, and biofilm thickness (L_F). Model predictions appear as solid line. Influent glucose observations are given by triangle symbol in part a while effluent glucose is given by solid circles. The standard error of estimate was approximately 15% for the L_F time series.

DOC and TOC were also measured but are not shown. Their average differed by less than 4% from that of the glucose influent concentration, indicating that glucose was the only component to be considered in the influent. Figure 1d shows the experimental and calculated biofilm thickness. The calculated values are obtained as the average of the biofilm thickness. The calculated values are obtained as the average of the biofilm thickness in all biofilm reactor segments. Considered in the simulation was the experimental observation that 4 days after inoculation a uniform biofilm appeared on the glass beads near the outside of the reactor. In general the correspondence between experimental and calculated time series is quite good.

Model Parameters

In Table I the model parameters used for the simulation are listed. Six parameters were given as experimental conditions. Twelve parameters, characterizing the biochemical reactions and physical properties of components and biofilm, were taken from the literature. The values of these parameters were deliberately not changed during the simulation, even though Figures 1b, c indicate that the calculated values of DOC and TOC are systematically too low toward the end of the experiment. A better fit of the experimental data was possible if the values of $Y_{psa/glu}$, $Y_{eps/glu}$, and k were increased. However, in order to keep the degrees of freedom for the simulation of the experiment as low as possible, the kinetics, stoichiometry, and parameter values of the biochemical reactions were left at the *a priori* values. Changes of D_{psa} and D_{eps} by two orders of magnitude did not have a visible effect on the calculated time series. Thus, estimates of the values of these parameters were used, making a total of 14 parameters which were held constant during the simulations.

Six model parameters in Table I were determined by a parameter fit. The initial conditions [i.e., $L_F(0)$ and $\epsilon_{s,psa}(0)$] have a visible effect on the calculated time series only during the first days of the experiment. For that time period the glucose removal rate depends mainly on the microbial mass in the reactor, $L_F A_{LF} \rho_{s,psa}$. The initial biofilm surface area is equal to the area of the reactor walls plus the total surface of the glass beads. The initial volume fraction of the attached cells, $\epsilon_{s,pes}(0)$, can vary only little, because the volume fractions must fulfill the condition

$$\epsilon_{s,psa} + \epsilon_{s,eps} + \epsilon_l = 1 \qquad (24)$$

Table I. Values of model parameters used for simulation of experiment.

Parameter	Symbol	Value	Units	Source
Flow rate	O	0.055	$m^3\ d^{-1}$	experiment
Reactor bulk fluid volume	V_c	1.43×10^{-5}	m^3	experiment
Influent Glucose concentration	$C_{in,glu}$	7 to 12	$g\ C\ m^{-3}$	experiment
Influent DO concentration	C_{in,O_2}	9	$g\ O_2\ m^{-3}$	experiment
Influent cell concentration	$X_{in,psa}$	0	$g\ C\ m^{-3}$	experiment
Influent eps concentration	$X_{in,eps}$	0	$g\ C\ m^{-3}$	experiment
Glucose diffusivity	D_{glu}	5.18×10^{-5}	$m^2\ d^{-1}$	[a]
Dissolved oxygen diffusivity	D_{O_2}	1.56×10^{-4}	$m^2\ d^{-1}$	[a]
Biofilm diffusivity/pure water diffusivity	f	0.8	—	[b]
Cell density	ρ_{psa}	1.2×10^5	$g\ C\ m^{-3}$	[c]
Eps density	ρ_{eps}	1.2×10^5	$g\ C\ m^{-3}$	[c]
Maximum specific growth rate	μ_{max}	9	d^{-1}	[d]
Glucose half-saturation coefficient	K_{glu}	2	$g\ C\ m^{-3}$	[e]
Oxygen half-saturation coefficient	K_{O_2}	0.2	$g\ O_2\ m^{-3}$	[f]
Cell yield coefficient	$Y_{psa/glu}$	0.34	$g\ C_{psa}\ g\ C_{glu}^{-1}$	[g]
Eps yield coefficient	$Y_{eps/glu}$	0.56	$g\ C_{eps}\ g\ C_{glu}^{-1}$	[g]
Stoichiometric coefficient	k	0.27	$g\ C_{eps}\ g\ C_{psa}^{-1}$	[e]
Stoichiometric coefficient	i_1	0.9	$g\ C\ g\ O_2^{-1}$	[h]
Cell diffusivity (in water)	D_{pes}	1×10^{-4}	$m^2\ d^{-1}$	estimate
Eps diffusivity (in water)	D_{eps}	1×10^{-4}	$m^2\ d^{-1}$	estimate
Initial biofilm thickness	$L_f(0)$	1×10^{-8}	m	par. fit
Initial volume fraction biofilm cells	$\epsilon_s(0)$	0.189	—	par. fit
Biofilm liquid phase volume fraction	ϵ_l	0.76	—	par. fit
Mass transfer resistance coefficient	λ	Fig. 2a	m	par. fit
Biofilm surface area	A_{LF}	Fig. 2b	m^2	par. fit
Detachment velocity	u_{de}	Fig. 2c	$m\ d^{-1}$	par. fit

[a]Ref. 2, p. 788.
[b]Ref. 3, p. 118.
[c]Ref. 1, p. 1422.
[d]Ref. 3, p. 247.
[e]Ref. 17, p. 1412.
[f]Ref. 9, p. 38.
[g]Ref. 17, p. 1414.
[h]Ref. 3, p. 189.

and the biofilm liquid phase volume fraction ϵ_l is large and can be determined relatively precisely. The strong increase of the biofilm thickness between the 4th and 10th day of the experiment is very sensitive to ϵ_l. The parameters $\epsilon_{s,\mathrm{psa}}(0)$ and $\epsilon_{s,\mathrm{eps}}(0)$ were calculated based on Equation (24) and on the assumption that $\epsilon_{s,\mathrm{psa}}(0)/\epsilon_{s,\mathrm{eps}}(0)$ is equal to the stoichiometric ratio $1/k$, at which cells and eps are produced. The parameters $\epsilon_{s,\mathrm{psa}}(0)$ is not included in Table I because according to equation (24) its value is fixed once $\epsilon_{s,\mathrm{psa}}(0)$ and ϵ_l are given. As shown in Figure 2, the values of the parameters λ, u_{de}, and A_{LF} change significantly during the course of the experiment.

Mass Transfer Resistance and Biofilm Surface Area

Figure 2a shows that the coefficient of mass transfer resistance at the biofilm–bulk fluid interface, λ, initially is 400 μm. This value is in the order of the radius of the glass beads (500 μm). This could mean that biofilm growth initially takes place around the sheltered contact points of the glass beads and that the cells are eroded preferentially in those areas of the glass beads' surface which are exposed to the current. This hypothesis is consistent with visual observations reported by Cunningham et al.[7] By day 4, when biofilm accumulation has become significant, λ begins to decrease, and by day 9, it is down at 20 μm. The explanation is that biofilm growth results in a decrease of the void space between the glass beads and, for a constant flow system, in an increase of the average pore velocity (Fig. 3). These changes cause alterations in both the flow pattern in the reactor and the mass transfer resistance at the interface between biofilm and bulk fluid. The biofilm surface area A_{LF} drops from its initial value of 0.1450 m^2 to about 0.025 m^2 at the end of the experiment. The explanation is that the biofilm does not grow evenly on the available solid surface but first fills up the "dead zones" between the glass beads, as is depicted in Figure 4. Thus, in the quasi-steady-state situation at the end of the experiment stream tubes are either clogged or their radius has become very small.

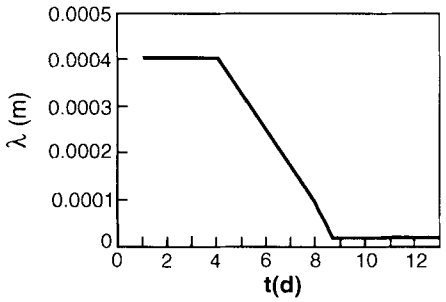

Fig. 2a Mass transfer resistance coefficient

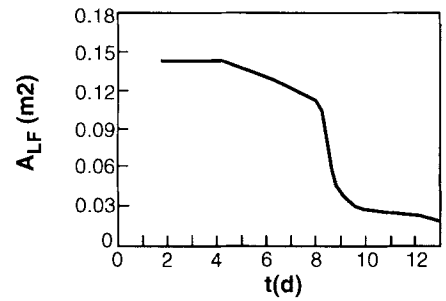

Fig. 2b Total biofilm surface area

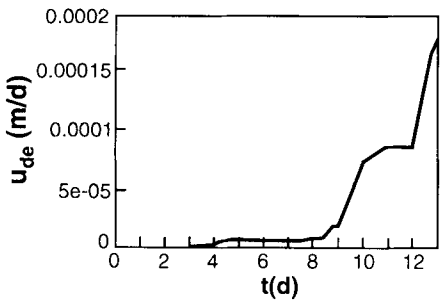

Fig. 2c Detachment velocity

Figure 2. Time series for mass transfer resistance coefficient (λ), biofilm surface area (A_{LF}), and detachment velocity (u_{de}) generated by parameter fitting routine in AQUASIM.

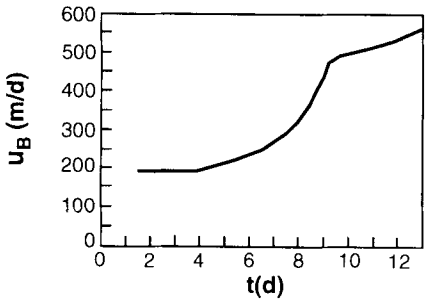

Figure 3. Time series for average pore velocity (u_B) calculated by AQUASIM.

The empirical functions $\lambda(t)$ and $A_{LF}(t)$ represent only a very rough description of reality. However, these functions show that three phases can clearly be distinguished during the experiment: an initial phase, a growth phase, and a mature biofilm phase. The simulation shows that in the initial phase the substrate removal rate, i.e., the flow rate times the difference between the substrate influent and effluent concentrations in Figure 1a, is very sensitive to the *P. aeruginosa*. biofilm thickness L_F (Fig. 1d) and to the mass transfer resistance between biofilm and bulk fluid. In the initial phase the effect of the biofilm on the flow in the bulk fluid is negligible. In the growth phase the substrate removal rate is sensitive to both the mass transfer resistance and the area of the biofilm–bulk fluid interface. In the mature biofilm phase, wherein the biofilm thickness has substantially reduced the free pore space, the substrate removal rate is very sensitive to the interfacial area, but not to the mass transfer resistance and the biofilm thickness. This may explain why our one-dimensional biofilm model, which can only approximate the complex geometry of a porous medium, is able to adequately reproduce the microbial growth and substrate removal observed in the experiment.

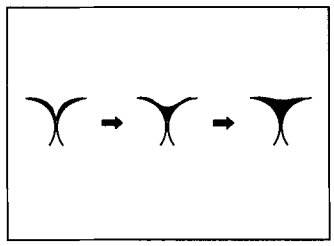

Figure 4. Assumed progression of biofilm accumulation in porous media.

In Figure 1a on day 9 the effluent glucose concentration drops sharply (to a minimum of approximately 2 g C m^{-3}) while the influent concentration remains relatively constant. This condition represents the highest substrate utilization rate observed during the experiment. Since glucose, DOC, and TOC were measured independently, this condition cannot be readily attributed to analytical error. The analysis of the simulation results reveals that this minimum originates from the changes of the mass transfer resistance coefficient λ and of the biofilm surface area A_{LF} (Figs. 2a, b). The decrease of λ causes the glucose concentration in the bulk fluid to be lowered. The corresponding decrease of A_{LF} causes the glucose concentration to increase. However, because the decrease of A_{LF} takes place later late than the decrease in λ, a minimum glucose concentration results on day 9.

Detachment

Since attachment is not explicitly considered in the model, u_{de} represents the net velocity at which *P. aeruginosa* cells and eps are detached from the biofilm surface into the bulk fluid. The parameter u_{de} can be quantified precisely by the simulation and the available experimental data since it directly affects the time series of both the biofilm thickness and TOC in the reactor effluent. Figure 2c shows $u_{de}(t)$ as it was obtained by the parameter fit. During the first 4 days u_{de} is very small. During the growth phase, between days 4 and 9, u_{de} is still relatively small and almost constant, (i.e., cells and eps are eroded from the biofilm surface at a constant rate during that time period). Between days 9 and 10, u_{de} linearly increases by a factor of 10, then remains stable until day 12. This pattern correlates with the measured pressure drop (Fig. 5a). Between days 12 and 13 there is another strong increase of u_{de}. This increase is explained by the change of the glucose influent concentration from about 8 to 16 g C m^{-3}, which triggered additional biofilm growth and possibly sloughing and clogging.

The simulation offers the opportunity to conduct a non-steady-state analysis of the detachment process by correlating the empirically formed function $u_{de}(t)$ with other parameters and variables. The variables plotted in Figures 5b, c were suggested by Peyton et al.[11] in a literature review of biofilm detachment functions. Figure 5b shows the correlation between L_F and u_{de}. The Figure confirms that u_{de} first is negligibly small and during the growth phase until day 8 is almost independent of L_F. Between days 8 and 9 there is an approximately linear relationship, then u_{de} increases further even if L_F remains almost constant. Similar patterns were found for the average pore velocity (Fig. 5c), along with other variables recommended by Peyton including glucose removal rate, glucose removal rate times biofilm thickness, and biofilm thickness squared. Thus no simple relationship was observed between u_{de} and these variables which are commonly related to biofilm detachment in var-

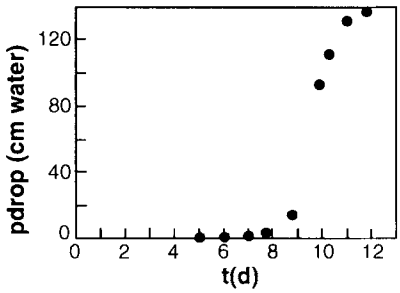

Fig. 5a Pressure drop

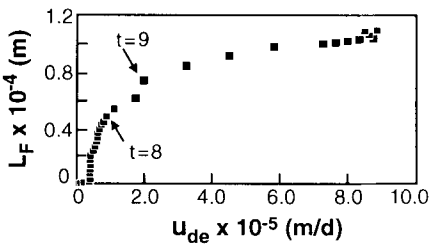

Fig. 5b Biofilm thickness vs. u_{de}

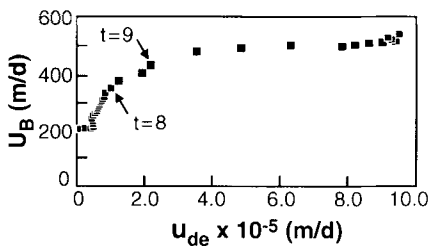

Fig. 5c Average pore velocity vs. u_{de}

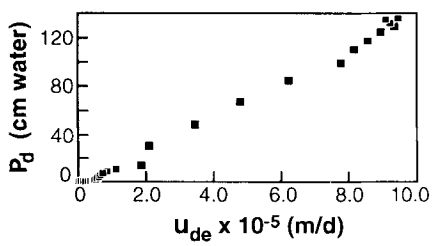

Fig. 5d Pressure drop vs. ude

Figure 5. Measured pressure drop time series in experimental system (5a), along with correlations between detachment velocity (u_{de}) and biofilm thickness (L_F), average pore velocity (u_B), and pressure drop (P_d).

ious types of flowing systems. However, an almost linear relationship between the measured pressure drop and u_{de} is seen in Figure 5d, indicating that in a porous medium under high substrate loading, detachment is highly correlated with shear at the biofilm surface.

Validity and Accuracy of Model

Spatial Discretization

Ten grid points were used to calculate the one-dimensional spatial gradients in the biofilm. Twelve grid points did not visibly change the calculated time series (maximum relative error <2%). The model as given by Equations (5) and (6) cannot model diffusion in the bulk fluid. The diffusion observed in the simulation results from the rough spatial discretization in the flow direction by only three biofilm reactor compartments. If the number of reactor compartments is increased, mass transport in the reactor becomes purely advective. The time series for glucose, DOC, TOC, and L_F obtained by a simulation alternatively performed with three and five segments did not show visible differences (maximum relative error <4%). Thus the reactor model used here may be applied given that the influent concentrations are varying slowly.

Tracer Experiment

During day 12 a pulse of sodium chloride was injected at the influent port of the reactor. Those data were used as input for a simulation which was based on nine reactor segments. The simulation was performed with the parameter values as listed in Table I (i.e., no parameter fit was made for this experiment). Comparison of the measured and calculated conductivity at the effluent port reveals that the average pore velocity is predicted quite well by the simulation, however, the diffusion as observed in the experiment is not reproduced adequately (Fig. 6). A simulation with no mass transfer resistance at the biofilm–bulk fluid interface and a several- fold increased diffusivity of the tracer in the biofilm did not significantly attenuate the maximum of the calculated pulse. Thus, the segmented reactor model cannot be applied for pulse inputs.

Biochemical Reactions

Maintenance and endogenous metabolism are not explicitly considered in this model. Thus, μ_{max} is a net maximum specific growth rate. The simulation revealed that an oxygen limitation in the biofilm is not predicted, other than for day 13 when the glucose influent concentration was substantially increased. If dissolved oxygen is not treated as a state variable (i.e., is kept constant over time and space in the reactor), the calculated time series do not change significantly, not even at day 13 (maximum relative error <5%). In conclusion, for the combinations of $C_{in,glu}$ and

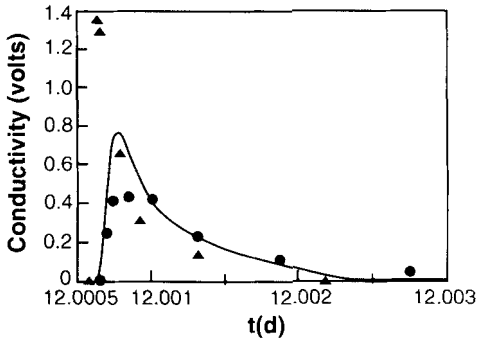

Figure 6. Comparison of influent and effluent salt tracer concentrations. Triangles represent tracer influent, solid circles represent measured effluent concentrations, and AQUASIM predictions are represented by the solid line.

C_{in,O_2} used in this experiment, gradients of dissolved oxygen do not have to be considered and the values of the parameters K_{O_2} and i_1 cannot be verified or corrected by the simulation.

CONCLUSIONS

Conventional one-dimensional advection–diffusion–adsorption models for porous media can be coupled with biofilm models.

For the accumulation of thick biofilms in porous media three phases can be distinguished: (1) an initial phase in which substrate removal is determined by cell mass and mass transfer resistance between biofilm and bulk fluid; (2) a growth phase in which cell mass, mass transfer resistance, and area of the biofilm–bulk fluid interface are important; and (3) a mature biofilm phase in which the area of the interface is the important parameter. In this phase mass transfer resistance between biofilm and bulk fluid is insignificant. The extent of biofilm accumulation in the porous medium determines the approach for modeling of the biofilm. For a mature-phase biofilm the biofilm thickness has little effect on the substrate removal rates. Thus, a one-dimensional biofilm model is able to adequately reproduce the microbial growth and substrate utilization observed in the experiment.

In a porous medium under high substrate loading biofilm detachment is correlated with shear at the biofilm surface.

This research was supported by the National Science Foundation (Cooperative Agreement EEC-8907039 with Montana State University). Although the research described in this article has been funded in part by the U.S. Environmental Protection Agency under assistance agreement R-815709 to Montana State University through the Hazardous Substance Research Center for U.S. EPA Regions 7 and 8 headquartered at Kansas State University, it has not been subjected to the Agency's peer and administrative review and, therefore, may not necessarily reflect the views of the Agency, and no official endorsement should be inferred.

References

1. Bakke, R., Trulear, M. G., Characklis W. G. 1984. Activity of *Pseudomonas aeruginosa* steady state biofilms. Biotechnol. Bioeng. **26**: 1418–1424.

2. Bennett, C. O., Myers, J. E. 1982. Momentum, heat and non transfer, McGraw-Hill, New York.
3. Characklis, W. G., Marshall, K. C. 1990. Biofilms. Wiley New York.
4. Chen, B., Cunningham, A., Ewing, R., Peralta, R., Visser, E. 1994. Two-dimensional modeling of microscale transport and biotransformation in porous media. Numer. Meth. Partial Diff. Eq. **10**: 65–83.
5. Cohen, Y., Metzner, A. B. 1981. Wall effects in laminar flow of fluids through packed beds. AICHE J. **27**(5):705–715.
6. Cunningham, A. B., Bouwer, E. J., Characklis, W. G. 1990. Biofilms in porous media, p. 697 In: W. G. Characklis and K. C. Marshall(eds.), Biofilms. Wiley, New York.
7. Cunningham, A. B., Characklis, W. G., Abedeen, F., Crawford, D. 1991. Influence of biofilm accumulation on porous media hydrodynamics. Env. Sci. Technol. **25**: 1305–1310.
8. Gujer, W., Wanner, O. 1990. Modeling mixed population biofilms. In: Biofilms. Characklis and Marshall (eds.), Wiley, New York, pp 397-445.
9. Lewandowski, Z., Walser, G., Characklis, W. G. 1991. Reaction kinetics in biofilms. Biotechnol. Bioeng. **38**: 877.
10. Okubo, T., Matsumoto, J., 1983. Biological clogging of sand changes of organic constituents during artificial recharge. Wat. Res., **17**(7): 813–821.
11. Peyton, B. M., Skeen, R. S., Hooker, B. S., Lundman, R. W., Cunningham, A. B. 1995. Evaluation of bacterial detachment rates in porous media. Appl. Biochem. Biotechnol., to appear.
12. Raiders, R. A., McInerney, M. J., Revus, D. E., Torbati, H. M., Knapp, R. M., Jenneman, G. E. 1986. Selectivity and depth of microbial plugging in Berea sandstone cores. J. Ind. Microbiol. **1**: 195–203.
13. Reichert, P. 1994. AQUASIUM—a tool for simulation and data analysis of aquatic systems. Water Sci. Tech. **30**(2):21–30.
14. Reichert, P. 1994b. Concepts underlying a computer program for the identification and simulation of aquatic systems. Schriftenreihe der EAWAG Nr. 7. Swiss Federal Institute for Environmental Science and Technology (EAWAG), Dübendorf, Switzerland.
15. Rittmann, B. E. 1993. The significance of biofilms in porous media. Water Resourc. Res. **29**(7):2195–2202.
16. Rittmann, B. E., McCarty, P. L. 1980. Model of steady state biofilm kinetics. Biotechnol. Bioeng. **22**: 2343–2357.
17. Robinson, J. A., Trulear, M. G., Characklis, W. G. 1984. Cellular reproduction and extracellular polymer pormation by *Pseudomonas aeruginosa* in continuous culture, Biotechnol. Bioeng. **26**: 1418–1424.
18. Saez, P. B., Rittmann, B. E. 1988. Accurate pseudoanalytical solution for steady-state biofilms. Biotechnol. Bioeng. **32**: 379.
19. Taylor, S. N., Jaffe, P. R. 1990. Biofilm growth and related changes in the physical properties of a porous medium 3. Dispersivity and model verification. Water Resourc. Res. **26**(9):2171–2180.
20. Trulear, M. G., Characklis, W. G. 1982. Dynamics of biofilm processes. J., Water Pollut. Control Fed. **54**(9):1288–1301.
21. Wanner, O. 1994. Modelling of mixed-population biofilm accumulation. In: C. G. Geesey, Z. Lewandowski, and H. C. Flemming (eds.), *Biofouling and Biocorrosion in industrial Water Systems*. Lewis, Ann Arbor, MI.
22. Wanner, O., and Gujer, W. 1986. A multispecies biofilm model. Biotechnol. Bioeng. **28**: 314–328.